BUILD SIMUL (2015) 8: 167 – 178
DOI 10.1007/s12273-014-0200-9

Effect of heat loads and ambient conditions on thermal comfort for single-sided ventilation

David Park, Francine Battaglia (✉)

Department of Mechanical Engineering, Virginia Tech, Blacksburg, VA 24061, USA

Abstract

Natural ventilation is an effective method to save energy required to condition buildings and to improve indoor air quality. Designing a naturally ventilated building is a greater challenge than designing a mechanically ventilated building because natural ventilation highly depends on weather, which changes continuously. Another factor that may alter air movement and thermal conditions in the building is the presence of heat loads and furniture. The objective of the current study is to examine the effects of various environmental conditions and room configurations on both airflow distribution and thermal conditions in a room. In this study computational fluid dynamics (CFD) was used to model single-sided buoyancy-driven ventilation in a room with a door. Experimental and numerical data from the literature were used to initially validate the CFD, and the results agreed fairly well. Various heat loads and furniture were added to the room to examine their effects on airflow stratification and thermal conditions. Overall, the conditions in a room were not significantly affected by additional heat sources. Lastly, cooler ambient conditions at the doorway were modeled, and the room was unable to achieve comfortable thermal conditions.

Keywords

single-sided ventilation,
natural ventilation,
thermal comfort,
building energy

Article History

Received: 25 June 2014
Revised: 14 September 2014
Accepted: 16 September 2014

1 Introduction

Energy consumption is an important issue and has become a great concern during the last few decades. World energy consumption has increased from 348.4 to 523.9 quadrillion Btu from 1990 to 2010, and the energy demand is projected to increase at a rate of 1.8% per year according to U.S. Energy Information Administration (2013). Building energy utilization accounts for a large portion of overall energy consumption. Most building energy is used for space heating and cooling purposes, and comprising 51% of energy consumption in residential buildings according to the annual review by U.S. Department of Energy (2008). One method of saving energy costs required for buildings is the use of natural ventilation, which supplies and removes air to the building without using mechanical ventilation systems. Natural ventilation has significant potential to reduce operating costs to condition buildings while maintaining acceptable indoor air quality. Emmerich et al. (2001) mentioned that office buildings in the United Kingdom saved cooling loads of 14 to 41 kWh/m^2 by using natural ventilation, which represented a 10% annual energy saving. Feng et al. (2008) showed that the potential energy savings in office buildings was approximately 30%. Brodrick and Westphalen (2001) indicated the growing trend of using fan power, which makes natural ventilation more attractive.

There are two types of natural ventilation: wind-driven ventilation and buoyancy-driven ventilation, and occur by wind and buoyancy forces, respectively. The buoyancy forces are induced from density gradients due to temperature gradients. The airflow and thermal conditions in the building can be altered by heat loads such as fires, electronic components, electrical heaters, and even from people. The two main ventilation principles are cross- and single-sided ventilation. Cross-ventilation is usually used for cooling purposes, and relies on wind to transport the cool air into an inlet (window, door, etc.) on one side of the room to transport the warm interior air through an outlet on the opposite side. Single-sided ventilation involves a room with openings on the same side. The temperature difference

E-mail: fbattagl@vt.edu

between the indoor and the outdoor environment creates a pressure difference, and the air is ventilated through an opening, where such buoyancy driven flow is also called the stack effect (Allocca et al. 2003; Larsen and Heiselberg 2008; RIBA 2014). The higher internal pressure occurs at upper section of the opening due to higher temperature, which drives outflow. The lower internal pressure at the lower section of the opening drives inflow.

Experiments are suited to study realistic natural ventilation airflow patterns, but it is expensive and time consuming. In addition, it is difficult to study the details of the airflow patterns in a building. Another method to model natural ventilation in a building is computational fluid dynamics (CFD), which is a numerical technique to solve the Navier–Stokes equations and predict the airflow within the building. In contrast to experimental methods, CFD is cost-effective and easy to investigate the effects of geometry changes on the flow. In addition, CFD provides spatial information giving values for variables such as pressure, temperature and velocity throughout the entire flow domain. CFD has great potential to become a powerful tool to model natural ventilation in buildings with careful and correct modeling of the problem. The main concern for CFD modeling is representing realistic flows. However, accuracy of CFD results compared to experimental studies has improved over the years. Allocca et al. (2003) showed that their CFD results for buoyancy-driven flows had a 10% difference compared to semi-analytical results, and 25% error for combined wind- and buoyancy-driven flow. Airflow rates for cross-ventilation were predicted within an error of 10%–15% using CFD by Cheuong and Liu (2011).

In this study, the commercial software ANSYS Fluent 12.1 is employed to model and study air stratification in a room with a large opening (single-sided ventilation) and a heater. The impetus for this study is to examine environmental conditions for office cubicles that do not have openings other than a door, where air quality and ventilation rates are important considerations. The current configuration represents a small room within a larger building, for example, multiple offices located along a corridor, where the ambient conditions may be considered as the hallway (indoor) conditions. The ratio between the height of the door to the room ceiling is roughly 0.7, whereas Allocca et al. (2003) used the ratio of 0.3 for their single-sided ventilation study. The results of Mahajan (1987) and Schaelin et al. (1992) are validated with the CFD results of this study. Appropriate boundary conditions are carefully chosen, and grid resolution and domain size studies are conducted to determine effective modeling of the problem. Furthermore, additional heat sources (e.g., computer, monitor and refrigerator) and furniture are considered to analyze their effects on overall air velocity and thermal conditions in the room. As previously mentioned, natural ventilation greatly depends on ambient conditions, and therefore another ambient temperature is tested to study the changes of airflow patterns and temperature in the room.

2 Background

2.1 Previous work

Studies have been performed to understand the physics of natural ventilation systems. Mahajan (1987) experimentally measured the heat and mass transfer through an opening, placed between two different thermally-conditioned rooms. The velocity and temperature measurements at the doorway (opening) were compared with values predicted by an algorithm based on the application of Bernoulli's equation. However, the analyses showed that the values from an algorithm did not agree well with the experimental results. Schaelin et al. (1992) utilized CFD and validated a model to predict a free plume and single-sided ventilation, modeling the work of Mahajan.

Several studies have been pursued using CFD for natural ventilation through buildings. Gan (2000) evaluated the effective depth of fresh air in rooms for single-sided buoyancy-driven ventilation and found that the effective depth of the room is affected by the width and height of the window opening, and room heat gains. Ravikumar and Prakash (2009) utilized CFD techniques to analyze thermal conditions in an office room with various window openings, and identified the optimum window opening area to maintain thermal comfort. Villi et al. (2009) developed a CFD model to study thermal performance of a wooden ventilated roof structure for different heights, and provided information describing the potential energy savings. Stoakes et al. (2011a, b) simulated natural ventilation flows in large, multistory buildings using the commercial software Fluent 6.0. They analyzed passive cooling and heating cases in the buildings, and showed the potential of CFD to model natural ventilation throughout whole buildings.

There are various studies that describe the effect of heat sources in a building using computational simulations. El-Agouz (2008) performed two-dimensional simulations to examine the effect of open locations for room ventilation with an internal heat source. A line heat source was placed on the floor, and multiple open locations were tested. It was found that indoor air quality was optimized by placing open locations on the ceiling. Cho and Awbi (2007) studied the effect of heat source locations on the mean room velocity using multiple regression analysis. They conducted experimental and numerical studies in a room with one inlet and one outlet. It was found that the mean velocity was lower when the heat source was located at the source of

the inflow. Kaye and Hunt (2010) predicted air stratification and ventilation rates in a room with two openings (at the bottom and upper surfaces) for heat sources of finite areas. They found that displacement ventilation flow was maintained when both room height and floor area were large compared to the size of the dominant heat sources, and when the effective vent area was relatively large, whereas it was difficult to maintain a stratified environment in rooms with low ceilings. Allocca et al. (2003) varied the heat loads from 0 to 1000 W in a room and observed an increase in air change rate per hour (ACH) with increasing heat loads.

The challenge of CFD is modeling realistic flows, particularly in the area of turbulence modeling and buoyancy-driven flow. The most common turbulence model is the k–ε model in which the turbulent kinetic energy, k, and turbulent dissipation rate, ε, are modeled. There are three types of k–ε turbulence models: standard k–ε, renormalization group theory (RNG), and realizable k–ε. The standard k-ε model is considered as the simplest two-equation turbulence model that solves two transport equations. The RNG model includes an additional term to improve the accuracy in the ε transport equation for rapidly strained flows and for swirling flows. The transport equation for ε is also modified for the realizable k–ε model to satisfy certain mathematical constraints on the Reynolds stresses.

Several studies have focused on turbulence models appropriate for natural ventilation. Chow and Li (2007) tested four turbulence models to study fire-induced thermal plumes: the standard k–ε, low-Reynolds number k–ε, Chen-Kim modified k–ε and RNG models. The authors found good agreement with experiments using the standard k–ε model while the other models did not give better results. Stavrakakis et al. (2008) experimentally and numerically investigated natural cross-ventilation in buildings. Three different turbulence models (standard, RNG, and realizable k–ε models) were tested. All turbulence models showed acceptable agreement with the experimental measurements, but overall differences were smallest for the standard k–ε model. Awbi (2003) mentioned that the standard k–ε model is the most used and developed turbulence model, and predicts airflow in buildings fairly well.

2.2 Single-sided ventilation

Single-sided ventilation is studied and representative velocity and temperature profiles at the doorway are shown in Figs. 1(a) and (b), respectively. The neutral level is defined as the point where gage pressure and velocity are zero, and separates the air inflow and outflow. Three different sections are identified for the temperature profile at the doorway: the constant temperature profile ($T = T_\infty$), the mixed layer temperature profile, and the constant temperature profile ($T = T_\infty + \Delta T$). The constant temperature profile below the mixed layer has a value equal to the ambient condition. The mixed layer profile is the section that shows a smooth transition from ambient temperature to the heated air temperature (from the heat sources); however, the mixed layer does not necessary start at the neutral level. The profiles shown in Fig. 1 serve as a reference for the validation study herein.

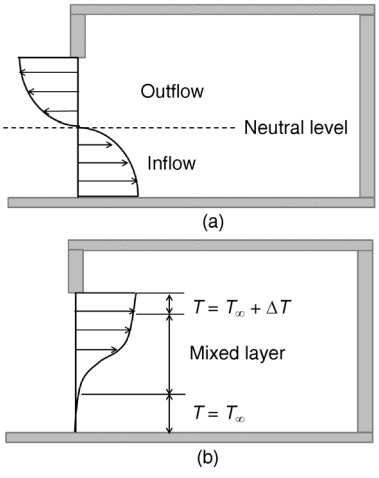

Fig. 1 Representative profiles for (a) velocity and (b) temperature in the doorway for single-sided ventilation

Another interest is to determine the effect of buoyancy forces on single-sided ventilation. There are two types of convective heat transfer, forced and free convection. The dominance of either forced or free convection effects can be determined by the ratio Gr/Re^2, where Gr is the Grashof number interpreted as the ratio of the buoyancy forces to the viscous forces and Re is the Reynolds number interpreted as the ratio of the inertia to viscous forces (Incropera et al. 2007). When the ratio is close to unity, both free and forced convection effects are important. If $Gr/Re^2 \gg 1$, buoyancy is dominant and if $Gr/Re^2 \ll 1$, buoyancy is negligible. In the current study, the Reynolds and Grashof numbers are calculated at the doorway using the relations:

$$Re = \frac{\rho \dot{V}}{\mu D_h} \tag{1}$$

$$Gr = \frac{g\beta \Delta T D_h^{\,3}}{\nu^2} \tag{2}$$

where in Eq. (1), ρ is the density, $\dot{V}$ is the volume flow rate, μ is the fluid dynamic viscosity, and D_h is the hydraulic diameter. In Eq. (2), g is gravity, β is the thermal expansion coefficient, ΔT is the temperature difference between the surface and ambient conditions, and ν is the kinematic viscosity.

2.3 Indoor air quality guidelines

Thermal comfort is determined by various factors to ensure indoor air quality. For the current study, only two factors are considered: air temperature and velocity. The recommended indoor temperatures by ASHRAE (2010) guidelines change according to ambient temperature. Two ambient temperatures of T_∞ = 22℃ and 10℃ are considered in the current study to represent the conditions in a building hallway or corridor. For T_∞ = 22℃, the maximum recommended temperature is 25℃, and the maximum acceptable temperature is 28℃. For T_∞ = 10℃, the maximum recommended and acceptable temperatures are 23 and 25℃, respectively. The minimum indoor temperature for T_∞ = 10℃ is 17℃.

Air velocity is also an important factor that determines the level of indoor thermal comfort. According to ASHRAE (2010), the maximum acceptable velocity is 0.8 m/s when $T_\infty > 25.5$℃ and the maximum acceptable velocity is 0.15 m/s when $T_\infty < 22$℃. For ambient conditions between 22℃ and 25.5℃, the maximum velocity allowed is determined by

$$v_{\text{maximum}} = 50.45 - 4.4047T_\infty + 0.096425T_\infty{}^2 \quad (3)$$

The recommended conditions by ASHRAE for two ambient conditions, 22℃ and 10℃, are summarized in Table 1.

Table 1 Recommended thermal conditions by ASHRAE (2010)

	T_∞ = 22℃	T_∞ = 10℃
$T_{\text{Recommended}}$ (℃)	22–25	19–23
$T_{\text{Acceptable}}$ (℃)	21–28	17–25
$V_{\text{Acceptable}}$ (m/s)	0.21	0.15

3 Numerical approach

3.1 Governing equations

The commercial software ANSYS Fluent (12.1) was used for all simulations. The following briefly presents the equations and models used in this work.

The equation for conservation of mass is

$$\frac{\partial \rho}{\partial t} + \vec{\nabla}\cdot(\rho\vec{v}) = 0 \quad (4)$$

where t is time and $\vec{v}$ is the velocity vector. Conservation of momentum is given by

$$\frac{\partial}{\partial t}(\rho\vec{v}) + \vec{\nabla}\cdot(\rho\vec{v}\vec{v}) = -\vec{\nabla}p + \vec{\nabla}\cdot\bar{\bar{\tau}} + \rho\vec{g} \quad (5)$$

where p is pressure, $\bar{\bar{\tau}}$ is the fluid stress tensor, and $\vec{g}$ is the gravitational vector. The fluid stress tensor for a Newtonian fluid is given by

$$\bar{\bar{\tau}} = \mu\left[\left(\vec{\nabla}\vec{v} + \vec{\nabla}\vec{v}^{\,\mathrm{T}}\right)\right] \quad (6)$$

The last term on the right hand side of Eq. (5) represents the buoyancy force. The Boussinesq model is employed to solve buoyancy-driven flows and assumes that density can be treated as a constant except in the buoyancy force term. The approximation is only valid when temperature differences are small so that density variations are very small. Relating changes of density and temperature, the thermal expansion coefficient, β, is defined as

$$\beta = -\frac{1}{\rho}\left(\frac{\partial\rho}{\partial T}\right)_{\mathrm{p}} \approx -\frac{1}{\rho}\frac{\rho_0 - \rho}{T_0 - T} \quad (7)$$

and the subscript 0 represents the reference value. Rearranging Eq. (7), the Boussinesq approximation can be represented as:

$$(\rho_0 - \rho) \approx \rho\beta(T - T_0) \quad (8)$$

Equation (8) is used to solve for ρ and substituted into the $\rho\vec{g}$ term of Eq. (5). The other ρ terms in Eqs. (4) and (5) are constant equal to ρ_0.

Conservation of energy is given by

$$\frac{\partial}{\partial t}(\rho E) + \vec{\nabla}\cdot[\vec{v}(\rho E + p)] = \vec{\nabla}\cdot k_{\text{eff}}\vec{\nabla}T + \vec{\nabla}\cdot(\bar{\bar{\tau}}_{\text{eff}}\cdot\vec{v}) + S_{\mathrm{h}} \quad (9)$$

where E is total energy and k_{eff} represents the effective conductivity, which considers the turbulent thermal conductivity in addition to fluid thermal conductivity. Viscous heating is also included, shown as the second term on the right hand side of Eq. (9).

3.2 Turbulence modeling

The standard k–ε turbulence model is used in this study, which assumes that the flow is turbulent and the effects of molecular viscosity are negligible. The turbulent kinetic energy, k, and its rate of dissipation, ε, in the flow field are calculated from two additional transport equations. The k–ε transport equations are

$$\frac{\partial}{\partial t}(\rho k) + \vec{\nabla}\cdot(\rho k\vec{v}) = \vec{\nabla}\cdot\left[\left(\mu + \frac{\mu_{\mathrm{t}}}{\sigma_\varepsilon}\right)\vec{\nabla}k\right] + G_{\mathrm{k}} + G_{\mathrm{b}} - \rho\varepsilon - Y_{\mathrm{M}} + S_{\mathrm{k}} \quad (10)$$

$$\frac{\partial}{\partial t}(\rho\varepsilon) + \vec{\nabla}\cdot(\rho\varepsilon\vec{v}) = \vec{\nabla}\cdot\left[\left(\mu + \frac{\mu_{\mathrm{t}}}{\sigma_\varepsilon}\right)\vec{\nabla}\varepsilon\right] + \rho C_1 S_\varepsilon + \rho C_2\frac{\varepsilon^2}{k + \sqrt{\nu\varepsilon}} - \rho\varepsilon + C_{1\varepsilon}\frac{\varepsilon}{k}C_{3\varepsilon}G_{\mathrm{b}} + S_\varepsilon \quad (11)$$

In these equations, G_k and G_b are the production of turbulent kinetic energy due to mean velocity gradients and buoyancy respectively; μ_t is the turbulent viscosity; $C_{1\varepsilon}$, $C_{2\varepsilon}$, and $C_{3\varepsilon}$ are also constants; and σ_k and σ_ε are turbulent Prandtl (Pr) numbers for k and ε respectively. The values of these parameters used by Fluent are: $C_{1\varepsilon}$ = 1.44, $C_{2\varepsilon}$ = 1.92, σ_k = 1.0, and σ_ε = 1.3. The coefficient $C_{3\varepsilon}$ determines the degree to which ε is affected by buoyancy and is calculated using a relationship between the velocity vector parallel and perpendicular to the gravitational vector. Further details can be found in the Fluent manual (Ansys 2009).

3.3 Numerical formulation

The semi-implicit method for pressure-linked equations (SIMPLE) is chosen to solve pressure-velocity coupling (Patankar 1980). The equations are integrated over a finite volume defined by a grid element and the dependent variables are solved at the center of each cell. From these cell-centered solutions, values at each face are interpolated using an upwind scheme. In the current study, momentum, energy and turbulent kinetic energy and dissipation rates are discretized using second-order upwind. For the gradient and pressure spatial discretization, least squares cell based (LSCB) and PRESTO! are applied, respectively. Time is discretized using a first-order implicit method. The Courant-Friedrichs-Levy (CFL) number of 1 is chosen to determine time step size:

$$\mathrm{CFL} = \frac{U\Delta t}{\Delta x} \tag{12}$$

where U is the maximum fluid velocity. The time step size and smallest cell size are expressed as Δt and Δx respectively. The absolute convergence criteria for the residuals are set to 10^{-5} except for the energy residual, which is set to 10^{-7}.

3.4 Boundary conditions

3.4.1 *Room with heater*

Figure 2 shows the computational domain and interior features including the heater for the representation of the room investigated in Mahajan (1987) and Schaelin et al. (1992). The room is 4.2 m long, 3 m high and 4 m wide, and the door is 0.12 m thick, 2.2 m high and 1 m wide. The heater (wall mounted radiator) is placed along the wall opposite the door, and is 0.12 m thick, 0.6 m high and 3 m wide. The thickness of the walls is also 0.12 m. The ambient conditions at the domain boundary are represented by specifying ambient pressure of 1 atm and temperature of 22℃ (additional cases will be discussed for different temperatures). For all cases, the heater radiates 50℃ of heat

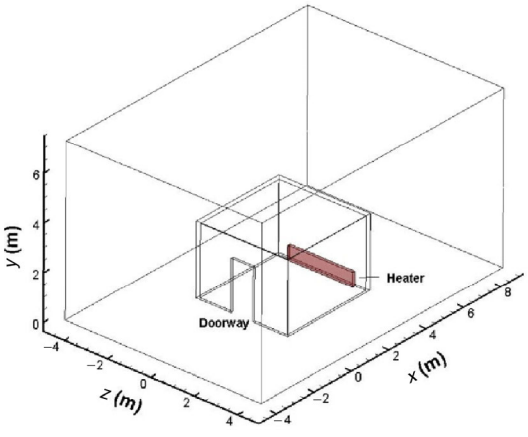

Fig. 2 Three-dimensional view of geometry for Domain A

to the room. The no-slip velocity boundary condition is applied for the fluid-wall interaction and the walls are modeled as adiabatic surfaces. The room with only a heater will be referred to as the "empty" room.

3.4.2 *Room with heater and furniture*

In a realistic room, there is more than just a heater, thus, additional furniture and heat sources are considered, where the layout in the room is shown in Fig. 3. The furniture and additional heat sources that can be commonly found in a typical office include a desk, chair, computer (hard drive), monitor, mini-refrigerator, and bookshelf. A desk is placed in front of the heater, which has dimensions 0.7 m × 0.65 m × 1.6 m in x, y, and z, respectively. The desk legs are 0.05 m thick in the x- and z-directions. The chair has dimensions 0.5 m × 0.95 m × 0.6 m and the legs are 0.05 m thick in the x- and z-directions. A computer hard drive is placed under the desk and has dimensions of 0.4 m × 0.5 m × 0.2 m. A monitor is placed on the middle of the desk and is 0.15 m × 0.4 m × 0.4 m. A storage box and a mini-refrigerator

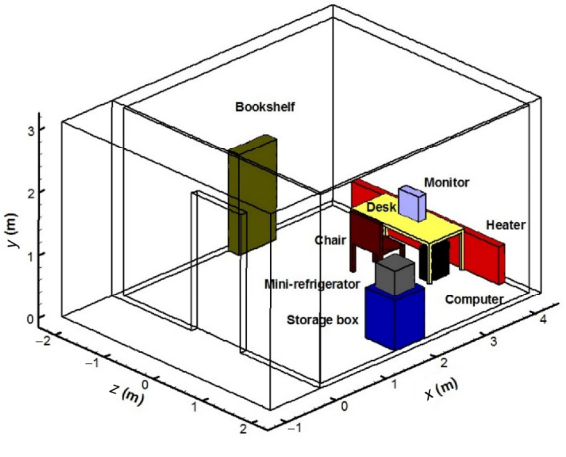

Fig. 3 Layout of furniture and heat sources in the room

are placed at the middle of the side wall. The storage box is 0.6 m × 0.8 m × 0.6 m and the mini-refrigerator is represented as a cube with a length of 4 m per side. A bookshelf is placed along the opposite wall and has dimensions of 0.22 m × 1.6 m × 0.75 m.

The computer hard drive and monitor have heat dissipation of 70 W and 35 W, respectively (invent hp 2007). The heat that dissipates from the mini-refrigerator is estimated using the coefficient of performance (COP) and the energy balance equation for the refrigeration system:

$$\mathrm{COP} = \frac{Q_{\mathrm{used}}}{W_{\mathrm{in}}} \tag{13}$$

where

$$Q_{\mathrm{dissipated}} = W_{\mathrm{in}} + Q_{\mathrm{used}} \tag{14}$$

The estimated energy consumption for a compact refrigerator is 348 kWh/yr, or approximately 40 W (Kenmore 2010) and the COP varies from 2.5 to 5. In this study, a COP of 3 is chosen and thus the mini-refrigerator approximately dissipates 120 W of heat. For each device, the heat dissipation normally occurs at the back of the device; thus, a heat flux is applied at the back of each device. No-slip and adiabatic boundary conditions are applied as boundary conditions along the back side. The heater is also turned on to produce warm air at 50℃. The room with a heater and furniture will be referred to as the "furniture" room.

3.5 Grid resolution study

The single-sided ventilation experiments of Mahajan (1987) are compared with the current simulations. For the experiments, two adjoining rooms were prepared under different conditions: one room was cooled to an average temperature of 19℃ to represent the ambient environment, and the other room was heated to an average temperature of 32℃. Thermostats were installed on the heater and air conditioning units to control the thermal conditions in each room. Measurements for velocity and temperature were sampled at the doorway connecting the rooms. The uncertainty of Mahajan's experiment was ± 0.025 m/s and ± 0.5℃ for the air speed and temperature measurements, respectively.

Simulations for the room with the heater were performed to determine the discretization error using the grid convergence index (GCI), as proposed by Roache (1994). In the current study, three grid resolutions were compared using uniform cell sizes of 3 cm, 6 cm and 12 cm for fine, medium and coarse grids, respectively.

In Fig. 4, the predicted velocity profiles at the doorway are compared with the experimental results from Mahajan (1987). The magnitude of the peak velocity below the neutral level increased slightly with decreasing grid spacing, and is in very good agreement with Mahajan's data. However, the peak velocity above the neutral level deviates from the experimental data and may be attributed to the uncertainty error in the experiment.

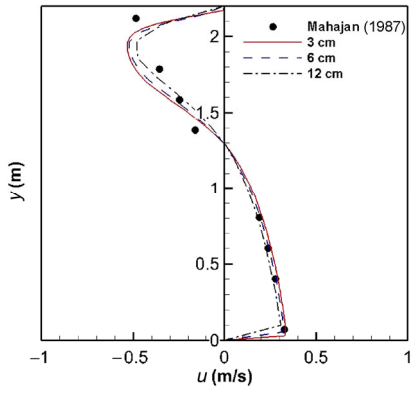

Fig. 4 Velocity profiles at the doorway for three different grid spacings and compared to Mahajan (1987)

The GCI is calculated using solutions from the three grid resolutions and is shown in Table 2 for the neutral level and peak velocities. The GCI for the finer grid (GCI_{21}) was relatively low compared to that for the coarser grid (GCI_{32}) showing that the grid refinement was successful. Low values of GCI indicate that the dependency of the numerical simulation on the cell size has been reduced. The largest GCI_{21} was 3.5% for the peak velocity above the neutral level. The GCI_{21} was less than 1% for the neutral level height and peak velocity below the neutral level. As shown in Fig. 4 and Table 2, the difference between solutions from the fine grid and medium grid was minor.

Using standard wall functions, dimensionless wall distance for the medium grid was investigated. It is recommended (Ansys 2009) that the adjacent wall cell centroid is placed within the log-law layer, $30 < y^+ < 300$. A uniform cell size was used even in the near-wall region and 5 cells are included in the boundary layer near the vertical and horizontal walls. The adjacent wall cell centroid is located between $40 < y^+ < 153$. For the purpose of saving CPU time as well as obtaining accurate numerical solutions, the medium grid resolution is used for the remainder of the study.

Table 2 GCI for three integration variables. Subscripts 1,2, and 3 represent fine, medium and coarse grid resolutions, respectively

	GCI_{32} (%)	GCI_{21} (%)
Neutral level Height (m)	0.13	0.20
Peak velocity (m/s) (above neutral level)	7.70	3.50
Peak velocity (m/s) (below neutral level)	3.10	0.76

4 Results and discussion

4.1 Empty room

The size of the domain is an important matter, especially for modeling airflow in large buildings, because a realistic representation of ambient and external airflow is essential. In addition, the size of the domain is related to grid resolution, which affects the CPU time. Thus, the study continues with a comparison of the predictions using three different domains. Schaelin et al. (1992) used a 3D domain of 34 m × 25 m × 18.7 m to computationally model the experiments of Mahajan (1987). However, the grid was not very fine having only 41 × 31 × 31 cells.

Three domain sizes are modeled here: Domain A, Domains B and C. Domain A includes the ambient environment around the room (Fig. 2), Domain B considers an ambient environment only in front of the doorway (Fig. 5(a)), and Domain C only deals with the room (Fig. 5(b)) where ambient conditions are incorporated as boundary conditions. Two-dimensional (2D) views of Domains B and C are shown in Fig. 5. There are 3 370 800, 342 433, and 278 462 cells in Domains A, B, and C respectively. Due to grid resolution and CPU constraints, Domain A will not be used for the remaining discussions. The time step size is 0.1 s and each case is simulated to 180 s.

Velocity and temperature profiles at the doorway are compared by using non-dimensional parameters for height, velocity and temperature, respectively:

$$H^* = \frac{y}{H} \tag{15}$$

$$u^* = \frac{u}{\sqrt{gH}} \tag{16}$$

$$T^* = \frac{T - T_\infty}{T_w - T_\infty} \tag{17}$$

where H is the height of the doorway, u is x-velocity, and T is temperature. The temperatures for the wall and ambient conditions are subscripted with w and ∞, respectively.

Non-dimensional velocity and temperature profiles are compared with Mahajan (1987) and Schaelin et al. (1992) in Fig. 6. The neutral level is identified when u^* equals zero and corresponds to $H^* = 0.1$ (Fig. 6(a)). Consistent with Mahajan, the velocity profile at the doorway is not symmetric with respect to the mid-height of the opening. Furthermore, the velocity magnitude of the outflow is larger than that of the inflow. Larger velocity magnitudes are predicted at the doorway for the simulations using Domains B and C. However, the neutral levels are well predicted, where the difference is 2.4% and 1.5% for Domains B and C, respectively. The neutral level predictions are summarized in Table 3.

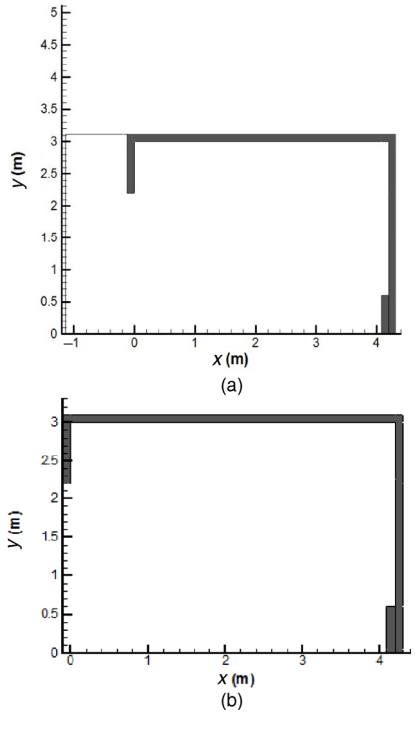

Fig. 5 Two-dimensional view of (a) Domain B and (b) Domain C (at z = 0 m)

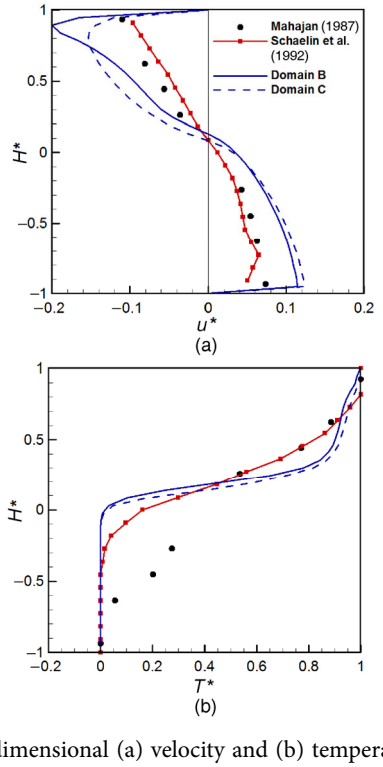

Fig. 6 Non-dimensional (a) velocity and (b) temperature profiles at the doorway: Mahajan (1987), Schaelin et al. (1992), and current simulations

Table 3 Neutral level predictions

	Neutral level (m)
Mahajan (1987)	1.21
Schaelin et al. (1992)	1.20
Domain B	1.24
Domain C	1.19

Examining Fig. 6 (b), the temperature profiles show good consistency with Schaelin et al. (1992), and agree fairly well with the experiment above $H^* = 0$. The consistency in solution profiles shows that standard k–ε turbulence model can also be used to predict stack effects. The discrepancies between the simulations (Schaelin et al. (1992) and the current work) and the experiments may be due to differences in modeling the ambient temperature. All simulations used $T_\infty = 22$℃ whereas the experiments controlled the "ambient" room at 19℃.

The Reynolds calculated using Eq. (1) for Domains B and C are Re = 23 600 and 24 800, respectively. The Grashof number using Eq. (2) is the same for both domains, where $Gr = 4.15 \times 10^9$. The ratio, Gr/Re^2 is 7.72 and 7.44 for Domains B and C, respectively, indicating that buoyancy dominates the flow distribution in the room. Additionally, the Re and Gr numbers for Domains B and C are similar, showing the effects of turbulence and buoyancy for single-sided ventilation can be predicted using a small domain such as Domain C.

4.2 Heat transfer through a large opening

Heat transfer rates for single-sided ventilation are discussed, where for these studies, the opening is the doorway. The heat transfer rate at the door can be calculated by integrating the product of velocity and temperature profiles over the height of the opening. The heat transfer rate per width across the opening (W/m) from ambient conditions to the room, q'_{in}, can be solved using (van der Mass 1992):

$$q'_{\text{in}} = C_{\text{d}} C_{\text{p}} \int_0^{y_{\text{n}}} \rho_0(y) u(y) T(y) \text{d}y \tag{18}$$

where y_{n} is the neutral level, and C_{d} is the coefficient of discharge, where a value of 0.7 is recommended by Schaelin et al. (1992). In the same manner, the heat transfer rate out of the room, q'_{out}, can be calculated by integrating from the neutral level to the height of the opening. Then, the total heat transfer rate is

$$q'_{\text{total}} = q'_{\text{in}} - q'_{\text{out}} \tag{19}$$

Heat transfer rates are summarized in Table 4 comparing the experiments and simulations. Heat transfer rates are different for all cases due to differences in magntidues of the velocity and temperautre profiles and also the height of the neutral level. The heat transfer rates (q'_{in} and q'_{out}) for the current simulations are greater than that for Mahajan (1987) due to larger velocity predictions at the doorway. Comparing total heat transfer rate through the doorway, the Schaelin et al. (1992) data give a smaller q'_{total} despite good agreement in velocity and temperature profiles with Mahajan (1987). Both current cases show good consistency in q'_{total} with Mahajan (1987), where q'_{total} for Domain C is larger than q'_{total} for Domain B. The neutral level is under-predicted by 1.5% for Domain C and thus Domain C predicts a relatively larger q'_{out} compared to q'_{in}.

Table 4 Heat transfer rates per width of the opening

	q'_{in}(kW/m)	q'_{out} (kW/m)	q'_{total} (kW/m)
Mahajan (1987)	55.2	66.2	−11.0
Schaelin et al. (1992)	50.3	53.4	−3.0
Domain B	103.7	115.6	−8.3
Domain C	108.8	122.9	−14.0

4.3 The effects of additional furniture and heat loads

Various heat sources and objects are added and modeled in order to analyze their effects on airflow and temperature distribution in the room. The empty room (only a heater), Fig. 5(a) for Domain B, and a room with furniture and additional heat sources (Fig. 3) are compared. Contours at various planes are shown in Fig. 7 to Fig. 10. Figures 7 (a) and (b) compare temperature contours with velocity vectors

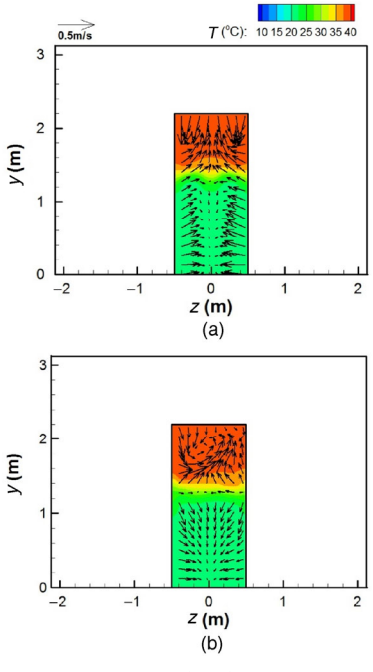

Fig. 7 Temperature contours with velocity vectors at the doorway (x = 0 m) for (a) empty and (b) furniture room for $T_\infty = 22$℃

in the *y-z* plane at the doorway (x = 0 m) for the empty and furniture rooms, respectively. Solutions are symmetric for the empty room due to the symmetric layout in the room, whereas the solutions with furniture are not symmetric. Interestingly, for the furniture room, air moves toward the bottom section of the doorway (y = 0.5 m and z = 0 m). The largest y-velocity occurs approximately at y = 1.7 m for each case at the doorway. Temperatures are uniformly stratified at the doorway in both cases.

Similarly, temperature contour with velocity vectors in the *y-z* planes at x = 1.8 m are plotted in Fig. 8, which cuts through the mini-refrigerator and the box. Air circulates at the bottom corners, where larger velocities can be noticed for the empty room. For the room with furniture, air circulation occurs in front of the storage box since that region protrudes from the wall. Temperature contours for the empty and furniture rooms are similar, except higher temperatures are noticeable behind the mini-refrigerator due to heat dissipation, which induces larger velocities.

Temperature contours with streamlines superimposed in the *x-y* plane at z = 0 m and z = 0.65 m are plotted in Fig. 9 and Fig. 10, respectively. The former and latter planes cut through the computer monitor and computer hard drive, respectively. As shown in Fig. 9, the ambient air enters the room, is heated (mostly by the heater), rises and exits through the doorway. A single circulation zone occurs for the empty room above the heater near the back wall (x = 3 to 4 m), whereas there is a larger circulation zone when furniture is present. The effect of heat transfer from the monitor is insignificant on temperature distribution since only 35 W of heat is dissipated.

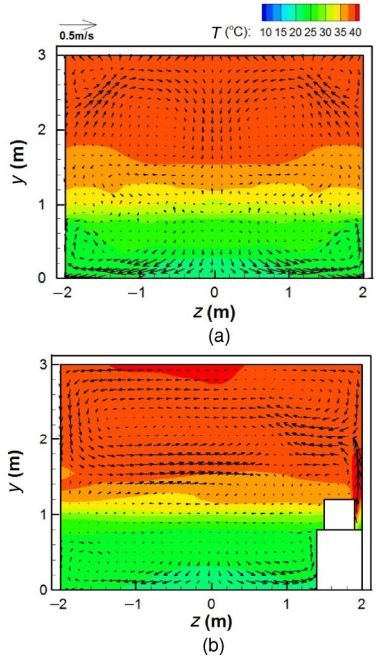

Fig. 8 Temperature contours with velocity vectors at x = 1.8 m for (a) empty and (b) furniture room for T_∞ = 22℃

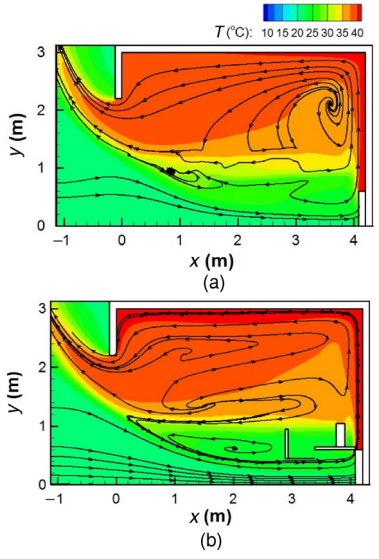

Fig. 9 Temperature contours with streamlines z = 0 m for (a) empty room and (b) furniture room for T_∞ = 22℃

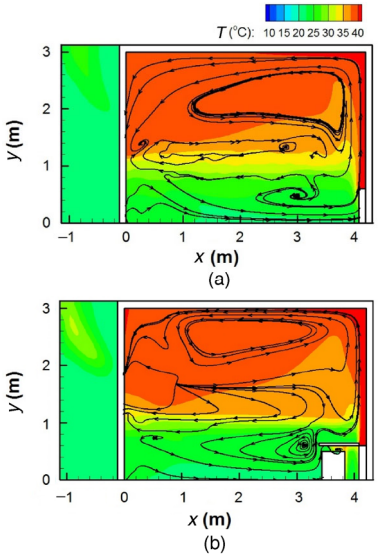

Fig. 10 Temperature with streamlines contours at z = 0.65 m for (a) empty room and (b) furniture room for T_∞ = 22℃

Figure 11 shows spatially averaged velocity magnitude and temperature along *x-z* planes at y = 1 m and 1.5 m for the empty and the furniture rooms for a 3-minute duration. The average velocity is slightly larger for the empty room than for the furniture room because the furniture impedes the motion of the air, slowing down the fluid velocity. The average velocity at y = 1.5 m is typically larger compared to that at y = 1 m since the density of air is lighter due to higher temperatures. The average velocity for both cases at each height does not exceed 0.21 m/s, which is the maximum acceptable velocity by ASHRAE (2010). Examining Fig. 11 (b), the average temperature for the first 90 s is slightly higher

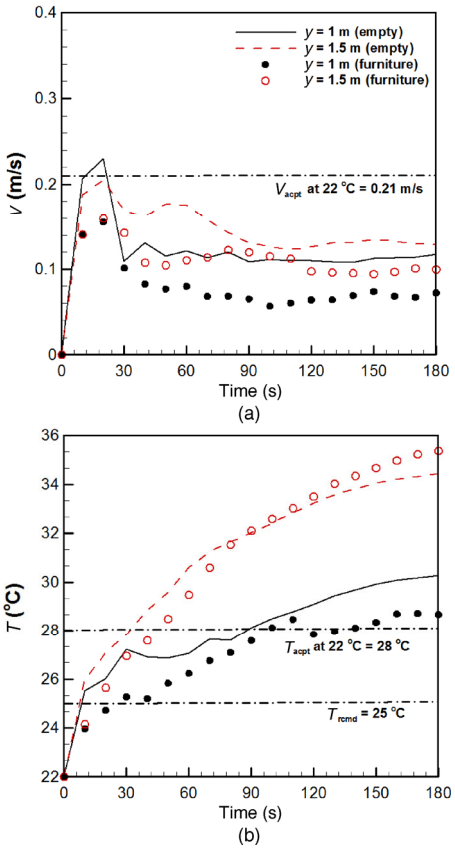

Fig. 11 Spatially averaged (a) velocity and (b) temperature at y = 1 m and 1.5 m for the empty and the furniture room with T_∞ = 22℃. Dashed dot lines show acceptable and recommended values from ASHRAE (2010) for T_∞ = 22℃

for the empty room than the furniture room. However, with more time, the effects of the additional heat loads in the furniture room increase the temperature at y = 1.5 m. The average temperatures in both room configurations reach 25℃, the maximum recommended temperature by ASHRAE, at approximately 15 s. The temperatures at y = 1 m and 1.5 m reach the maximum acceptable value at approximately 90 s and 45 s, respectively. Overall, significant differences between the empty room and furniture room were not noticeable comparing air velocity and temperature. The non-dimensional parameters were similar to the empty room, yet slightly larger, where Re = 22 942 and $Gr = 4 \times 10^9$, and the ratio Gr/Re^2 = 7.95, showing a small increase in buoyancy effects due to additional heat loads.

4.4 The effects of ambient temperature

Schaelin et al. (1992) modeled a room with a heater for a warm ambient temperature of 22℃ (refer to Section 4.2). Realistically, a heater is not usually turned on for such warm ambient air temperatures. In this section, the room is modeled with furniture at a cooler ambient temperature of 10℃, which is a more reasonable condition for the heater to be turned on.

Figure 12 shows temperature contours with velocity vectors at the doorway (x = 0 m) and x = 1.8 m with T_∞ = 10℃, which are compared to the results at T_∞ = 22℃ presented in the previous section (refer to (b) of Fig. 7 and Fig. 8). Similar to the results for the furniture room at T_∞ = 22℃ (refer to Fig. 7 (b)), the solutions are non-symmetric. Due to a lower ambient temperature, the overall temperature in the room is lower in Fig. 12. Larger velocities are noticeable for T_∞ = 10℃ compared to 22℃ due to larger temperature differences between the heat loads and surroundings. The ratio Gr/Re^2 is 11.7, indicating that the increasing fluid velocity in the room is largely due to an increasing buoyancy effect.

Figure 13 compares spatially-averaged velocity and temperature histories at y = 1 m and 1.5 m for the furniture room at T_∞ = 10℃ and 22℃. The overall average velocity for T_∞ = 10℃ is about twice as large as that for T_∞ = 22℃, and approximately 0.1 m/s faster than the recommended air velocity by ASHRAE when T_∞ < 22℃ (0.15 m/s). Due to larger temperature differences between the ambient environment and the room, greater pressure differences induce faster airflow rates at the opening. The average velocities for T_∞ = 10℃ at y = 1 m and 1.5 m are approximately 0.2 m/s and 0.25 m/s, respectively. The average temperature at y = 1 m and 1.5 m for T_∞ = 10℃ reaches the recommended temperature (23℃) by ASHRAE after 90 s and 60 s, respectively. The maximum acceptable temperature (25℃) is reached after 110 s and 90 s, respectively, which is not desirable for comfortable conditions.

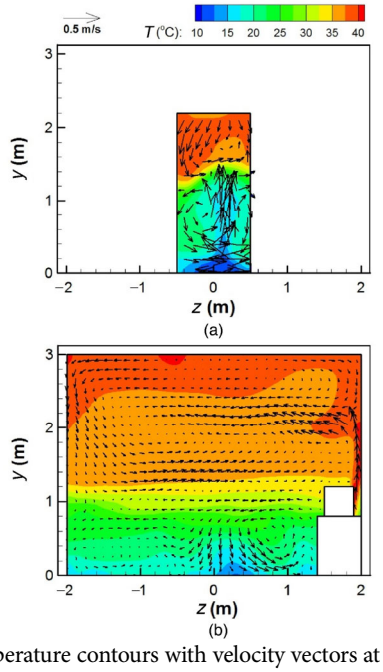

Fig. 12 Temperature contours with velocity vectors at (a) the doorway (x = 0 m) and (b) x = 1.8 m for furniture room with T_∞ = 10℃

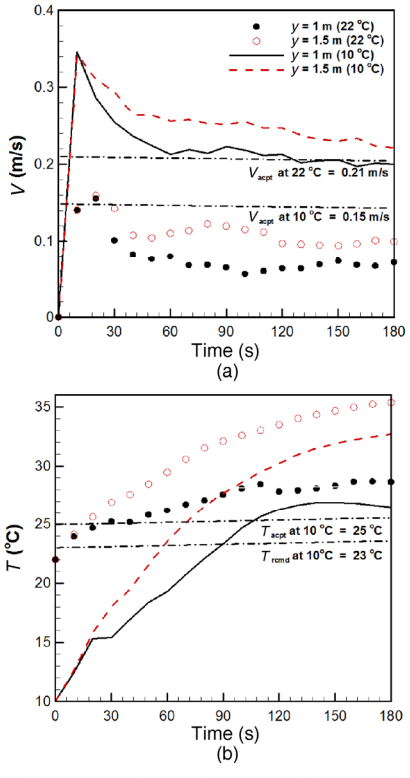

Fig. 13 Spatially averaged (a) velocity and (b) temperature at y = 1 m and 1.5 m for the furniture room at $T_\infty = 10℃$ and 22℃. Dashed dot lines show acceptable and recommended values from ASHRAE guideline for $T_\infty = 10℃$

Temperature contours with streamlines superimposed in 3D are shown in Fig. 14 for the empty and furniture cases at $T_\infty = 22℃$, and the furniture case at $T_\infty = 10℃$. Examining Fig. 14 (a), ambient air enters the room through the bottom of the dooway, which is heated by the heater at the opposite side. Then, the heated air rises and exits through the doorway. The effects of additional heat sources and furniture are difficult to observe in Fig. 14(b), where it shows similar temperatures and air movement through the doorway. More air mixing around the room can be noticed with the additional furniture (see Fig. 14 (b)). Examining Fig. 14 (c), the room temperature is much lower due to the cooler ambient temperature. The streamlines show that the air warmed by the heater exiting through the doorway does not significantly rises when $T_\infty = 10℃$ as it did for the case with $T_\infty = 22℃$.

The ACH is summarized in Table 5 for all cases (empty, furniture, and furniture with lower ambient temperature). The ACH is slightly larger for the empty room compared to the furniture room due to additional furniture impeding the flow velocity. Interestingly, ACH decreases for the lower ambient temperature, while the average velocity in the room increases (refer to Fig. 14). Although the ACH decreases for lower ambient temperature, the ventilation rate in a room with an opening is still effective, and is larger than the recommended ACH of 2–15 to remove heat (RIBA 2014).

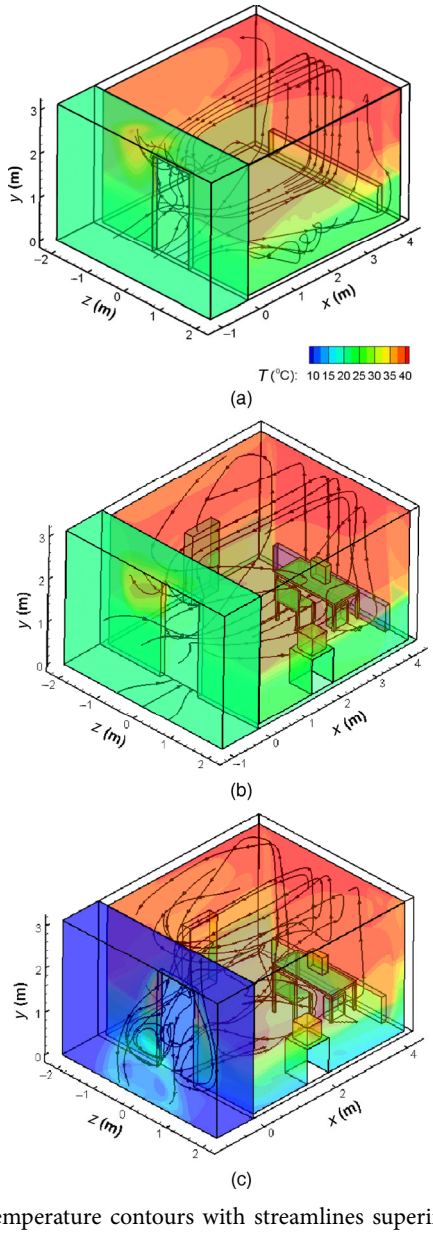

Fig. 14 Temperature contours with streamlines superimposed in 3D at t = 2 minutes for (a) empty at $T_\infty = 22℃$, (b) furniture at 22℃, and (c) furniture at 10℃

Table 5 Air change rate per hour (ACH) for empty and furniture at $T_\infty = 22℃$ and furniture at $T_\infty = 10℃$

	ACH
Empty ($T_\infty = 22℃$)	26.61
Furniture ($T_\infty = 22℃$)	26.55
Furniture ($T_\infty = 10℃$)	23.04

5 Conclusions

A single room with a door was analyzed using computational fluid dynamics. The predictions for velocity and

temperature profiles at the doorway were initially validated with the experiments and numerical solutions presented by Mahajan (1987) and Schaelin et al. (1992), respectively. The current CFD study modeled three different domain sizes to include the room and the ambient environment surrounding the room. Relatively small domains were used in this study compared to Schaelin et al. (1992), and the solutions at the doorway agreed fairly well with the experimental results from Mahajan (1987). The current work also showed that the standard k–ε turbulence model can be used to study stack effects at the opening by predicting the neutral level. Using the velocity and temperature profiles, the heat transfer rates were calculated at the doorway. It was found that the position of the neutral level was an important factor that affected the total heat transfer rate through the doorway.

The effects of additional heat sources and furniture were studied by comparing to the case with only a radiator (empty room) for $T_\infty = 22℃$. High temperatures and large velocities were predicted in the vicinity of the heat sources. Overall, velocity and temperature did not change significantly despite additional heat sources because the effect of the radiator was much greater than the other heat sources.

Lastly, the room with furniture was modeled with $T_\infty = 10℃$ to study the effect of ambient conditions. Larger velocities and lower temperatures occurred due to the cooler ambient temperature and also increased buoyancy effect. Spatially averaged velocity for $T_\infty = 10℃$ was approximately twice as large for $T_\infty = 22℃$. At $T_\infty = 10℃$, the average velocity was higher than the maximum acceptable velocity by ASHRAE , but the room was able to achieve the maximum recommended temperature within 3 minutes. The calculated ACH suggested that the buoyancy-dominated flow is still effective to remove heat and maintain good air quality levels in single-sided ventilation.

References

Allocca C, Chen Q, Glicksman LR (2003). Design analysis of single-sided natural ventilation. *Energy and Buildings*, 35: 785–795.

Ansys (2009). ANSYS FLUENT 12.0 User's Guide. Canonsburg, PA, USA: Ansys Inc.

ASHRAE (2010). ASHRAE Standard 55-2010 Thermal Environment Standards for Human Occupancy. Atlanta, GA, USA: American Society of Heating, Refrigerating and Air Conditioning Engineers.

Awbi HB (2003). Ventilation of Buildings, 2nd edn. London: Spon Press.

Brodrick JR, Westphalen D (2001). Uncovering auxiliary energy use. *ASHRAE Journal*, 43(2): 58.

Cheuong JOP, Liu CH (2011). CFD simulations of natural ventilation behaviour in high-rise buildings in regular and staggered arrangements at various spacings. *Energy and Buildings*, 43: 1149–1158.

Cho YJ, Awbi HB (2007). A study of the effect of heat source location in a ventilated room using multiple regression analysis. *Building and Environment*, 42: 2072–2082.

Chow WK, Li J (2007). Numerical simulations on thermal plumes with k–ε types of tubulence models. *Building and Environment*, 42: 2819–2828.

El-Agouz SA (2008). The effect of internal heat source and opening locations on environmental natural ventilation. *Energy and Buildings*, 40: 409–418.

Emmerich SJ, Dols WS, Axley JW (2001). Natural Ventilation Review and Plan for Design and Analysis Tools. National Institue of Standards Technology, NISTIR 6781.

Feng J, Xu Z, Jie Y (2008). Natural ventilation potential analysis of office building in China. *Journal of Tongji University*, 36(1): 92–96.

Gan G (2000). Effective depth of fresh air distribution in rooms with single-sided natural ventilation. *Energy and Buildings*, 31: 65–73.

Incropera FP, De Witt DP, Bergman TL, Lavine AS (2007). Fundamentals of Heat and Mass Transfer, 6th edn. New York: John Wiley and Sons.

invent hp (2007). Quickspecs. HP L1908w 19-inch Widescreen LCD Monitor.

Kaye NB, Hunt GR (2010). The effect of floor heat source area on the induced airflow in a room. *Building and Environment*, 45: 839–847.

Kenmore (2010). Compact Refrigerator: 46-94683/9. Sears Commercial.

Larsen TS, Heiselberg P (2008). Single-sided natural ventilation driven by wind pressure and temperature difference. *Energy and Buildings*, 40: 1031–1040.

Mahajan BM (1987). Measurement of interzonal heat and mass transfer by natural convection. *Solar Energy*, 38: 437–466.

Patankar SV (1980). Numerical Heat Transfer and Fluid Flow. New York: Hemisphere Publishing.

Ravikumar P, Prakash D (2009). Analysis of thermal comfort in an office room by varying the dimensions of the windows on adjacent walls using CFD: A case study based on numerical simulation. *Building Simulation*, 2: 187–196.

RIBA Royal Institue of British Architects (2014). Available at http://www.architecture.com/SustainabilityHub/Designstrategies/Air/1-2-1-2-Naturalventilation-stackventilation.aspx.

Roache PJ (1994). Perspective: A method for uniform reporting of grid refinement studies. *ASME Journal of Fluids Engineering*, 116: 405–413.

Schaelin A, Moser A, van der Mass J (1992). Simulation of airflow through large openings in buildings. *ASHRAE Transactions*, 98(2): 319–328.

Starakakis GM, Vrachopoulos MGr, Markatos NC, Koukou MK (2008). Natural cross-ventilation in buildings: Building-scale experiments, numerical simulation and thermal comfort evaluation. *Energy and Buildings*, 40: 1666–1681.

Stoakes P, Battaglia F, Passe U (2011a). Predicting natural ventilation flows in whole buildings. Part 1: The Viipuri Library. *Building Simulation*, 4: 263–276.

Stoakes P, Battaglia F, Passe U (2011b). Predicting natural ventilation flows in whole buildings. Part 2: The Esherick House. *Building Simulation*, 4: 365–377.

U.S. Department of Energy (2008). Annual Energy Review 2007.

U.S. Energy Information Administration (2013). International Energy Outlook 2013.

van der Mass J (1992). Air flow through large openings in buildings. Energy Conservation in Buildings and Community Systems Programme Annex 20 Technical Report (Subtask 2 : Air Flows between Zones).

Villi G, Pasut W, De Carli M (2009). CFD modeling and thermal performance analysis of a wooden ventilated roof structure. *Building Simulation*, 2: 215–228.